MATEMATIKA: MJIAM, Special Issue, December 2019, 33–52

Unsteady MHD Flow of Cassonnano Fluid with Chemical Reaction, Thermal Radiation and Heat Generation/Absorption

Nur Azlina Mat Noor, Sharidan Shafie and Mohd Ariff Admon*

Department of Mathematical Sciences, Faculty of Science, Universiti Teknologi Malaysia
81310 Skudai, Johor, Malaysia

*Corresponding author: ariffadmon@utm.my

Article history
Received: 11 November 2019
Received in revised form: 21 November 2019
Accepted: 23 December 2019

Published online: 31 December 2019

Abstract The hydromagnetic mixed convection flow of Cassonnano fluid under the influence of chemical reaction,thermal radiation and heat generation or absorption is investigated. The flow is induced due to unsteady nonlinearly stretching sheet saturated in a porous medium. The governing nonlinear coupled partial differential equations are converted into the system of coupled ordinary differential equations using similarity transformations and then solved numerically via Keller box method. The effects of pertinent parameters on velocity, temperature and nanoparticles concentration as well as wall shear stress, heat and mass transfer rate are analyzed and displayed graphically. The results for skin friction coefficient and local Nusselt number are compared with previously published work and found to be in good agreement. Findings demonstrate that increase in Casson parameter enhanced the friction factor and heat transfer rate. It is noticed that the heat transfer rate is declined with increment in Brownian motion and thermophoresis parameters. The nanoparticles concentration is seen to be higher in generative chemical reaction and opposite effect is observed in destructive chemical reaction. Increase in unsteadiness parameter decreased the fluid velocity, temperature and nanoparticles concentration. The magnitude of wall shear stress is also reduced with increase in unsteadiness and porous medium parameters.

Keywords Cassonnano fluid; stretching sheet; chemical reaction; thermal radiation; heat generation

Mathematics Subject Classification 76A05, 35Q35.

1 Introduction

Nanofluids are engineered colloids made of base fluid and nanoparticles. This new class of fluid was first discovered by Choi and Eastman [1]. They introduced a new class of heat transfer fluids created by suspending metallic nanoparticles in conventional heat transfer fluids. The resulting fluids known as nanofluids are expected to exhibit high thermal conductivities compared to

those base fluids. The nanoparticles used in nanofluids are made of metals (Al, Cu) or non-metals (Graphite, carbon nanotubes) and the base fluid is usually liquid such as water, kerosene oil or ethylene glycol. The thermal conductivity of nanofluids is greater than those base fluids because the suspended ultrafine particles significantly improve its capability in energy exchange [2]. Several researchers agreed that a small amount of nanoparticles volume fraction (5% or less) can enhance thermal conductivity of base fluid by more than 20%. These enhancements depend upon the shape of particles, dimensions of particles, thermal properties of particles, and volume fractions of suspended particles [3]. There are several general applications of nanofluids such as vehicle cooling, reducing fuel in electric power plant, cancer therapy, imaging and sensing. Wong and De Leon [4] pointed out that in cancer patients, iron-based nanoparticles can be used as delivery vehicles of drugs and radiation. Later on, Buongiorno [5] carried out analysis on nanofluids and deduced that outof seven slip mechanisms, only Brownian motion and thermophoresis are important mechanisms in nanofluids. It was found that Brownian motion and thermophoresis are responsible for heat transfer enhancement. Based on his predictions, he proposed a model which is known as Buongiorno's model. It is worth mentioning that several researchers have adopted Buongiorno's model in their study [6-8].

The study of boundary layer flow over a stretching sheet has gained attention due to its practical applications in several industries such as extrusion of plastic and rubber sheet, glass manufacturing, paper production, polymer processing and purification of crude oil. Crane [9] was the first who investigated the flow caused by stretching sheet, whose velocity is varying linearly from the fixed point. Numerous literatures are available on boundary layer flow of linear stretching sheet; however, the stretching sheet velocity need not be linear [10]. In view of this fact, researchers diverted their study to the boundary layer flow caused by exponential, quadratic and nonlinear stretching sheet. Keeping this in mind, Kumaran and Ramanaiah[11] examined fluid flow over quadratic stretching sheet. Magyari and Keller [12] analysed heat and mass transfer in the boundary layers past exponentially stretching sheet. Cortell[13] studied two-dimensional viscous flow caused by nonlinearly stretching sheet. Hsiao [14] reported the effect of thermal radiation on mixed convection flow over nonlinearly stretching sheet.

Most of the studies are limited to steady flow over a stretching sheet, yet sudden stretching of the sheet lead to occurrence of unsteady fluid flow. The unsteadiness cause changes in wall velocity or wall temperature. Sharidan *et al.* [15] studied similarity solutions of unsteady boundary layer flow caused by stretching sheet. Bachok *et al.* [16] analyzed unsteady boundary layer flow of nanofluid past a permeable stretching sheet. An analytical solution for unsteady boundary layer flow of nanofluid due to impulsive stretching sheet is investigated by Mustafa *et al.* [17]. The effects of Soret and Dufour on unsteady flow of Casson fluid over a nonlinearly stretching sheet with slip and convective boundary conditions is explored by Ullah *et al.*[18].

Casson fluid is classified as a non-Newtonian fluid due to its rheological characteristics in relation to the shear stress and strain relationship. The Casson fluid is a shear thinning fluid which exhibits yield stress and high shear viscosity. The Casson model was originally developed by Casson [19] for printing inks and silicon suspension. Common examples of Casson fluid are honey, jelly, soup, tomato sauce and concentrated fruit juices. In Casson fluid, Mukhopadhyay [20] studied boundary layer flow over nonlinearly stretching sheet. Sumalatha and Bandari [21] reported on boundary layer flow of Casson fluid due to nonlinearly stretching sheet in the influence of thermal radiation. Oyelakin *et al.* [22] examined unsteady MHD Cassonnano fluid generated by stretching surface in the presence of viscous dissipation, Soret

and Dufour, slip and convective boundary conditions. The study of MHD mixed convection flow of Casson fluid over an unsteady nonlinearly stretching sheet in a porous medium under the influence of chemical reaction, thermal radiation and heat generation/absorption is reported by Ullah *et al.* [23].

Motivated by the above cited papers, the objective of the present study is to investigate hydromagnetic mixed convection flow of Cassonnanofluid caused by nonlinearly stretching sheet embedded in a porous medium in the presence of chemical reaction, thermal radiation and heat generation or absorption. Further, the effect of viscous dissipation, joule heating, slip and convective boundary conditions are also considered. The governing equations are transformed to ordinary differential equation via similarity transformations and then solved numerically through the Keller-box method. The numerical algorithm for this problem is validated through comparison with existing literature results and excellent agreement is obtained. The physical behavior of pertinent parameters on fluid velocity, temperature and nanoparticles concentration are displayed and analyzed.

2 Mathematical Formulation

Consider an unsteady, two dimensional, incompressible mixed convection MHD flow of Cassonnanofluid generated by nonlinearly stretching sheet saturated in a porous medium under the influence of chemical reaction, thermal radiation and heat generation/absorption. Further, the effects of viscous dissipation, joule heating, slip and convective boundary conditions are also taken into account. The flow occupies the domain$y > 0$. The sheet is stretched in$x$ direction by keeping the origin fixed. Initially at $t \leq 0$ both the sheet and fluid are at rest and at the same temperature T_∞ and concentration C_∞. The sheet is suddenly stretched with the nonlinear velocity of the form$u_w(x,t) = cx^n/(1-\varepsilon t)$. Here $c > 0$, $\varepsilon \geq 0$ are constants, t is time and $n\,(>0)$ represents the nonlinearly stretching sheet parameter ($n = 1$ represents linear stretching sheet and $n \neq 1$ corresponds to nonlinear stretching sheet). The fluid is electrically conducted due to an application of magnetic field $B(x,t) = B_0 x^{(n-1)/2}(1-\varepsilon t)^{-1/2}$ normal to the sheet with constant B_0.

The rheological equation of a state for an isotropic and incompressible flow of Casson fluid is given by Pramanik [24] as

$$\tau_{ij} = \begin{cases} 2\left(\mu_B + p_y/\sqrt{2\pi_1}\right)e_{ij}, & \pi_1 > \pi_c, \\ 2\left(\mu_B + p_y/\sqrt{2\pi_c}\right)e_{ij}, & \pi_1 < \pi_c, \end{cases} \tag{1}$$

where μ_B is the dynamic viscosity of the non-Newtonian fluid, p_y is the yield stress of the fluid, π_1 is the product of the component of deformation rate with itself where $\pi_1 = e_{ij}e_{ij}$, e_{ij} is the $(i,j)^{th}$ component of the deformation rate and π_c is the critical value of this product based on the non-Newtonian model.

The governing equations of continuity, momentum, energy and concentration for Cassonnanofluid using the above assumptions with Boussinesq and boundary layer approximations are given as

$$\frac{\partial u}{\partial x} + \frac{\partial v}{\partial y} = 0, \tag{2}$$

$$\frac{\partial u}{\partial t}+u\frac{\partial u}{\partial x}+v\frac{\partial u}{\partial y}=\nu_f\left(1+\frac{1}{\beta}\right)\frac{\partial^2 u}{\partial y^2}-\frac{\sigma B^2(x,t)}{\rho_f}u-\nu_f\left(1+\frac{1}{\beta}\right)\frac{\varphi}{k_1}+g_x\beta_T(T-T_\infty)+g_x\beta_C(C-C_\infty), \tag{3}$$

$$\frac{\partial T}{\partial t}+u\frac{\partial T}{\partial x}+v\frac{\partial T}{\partial y}=\alpha_f\frac{\partial^2 T}{\partial y^2}+\tau\left[D_B\frac{\partial C}{\partial y}\frac{\partial T}{\partial y}+\frac{D_T}{T_\infty}\left(\frac{\partial T}{\partial y}\right)^2\right]+\frac{\nu_f}{c_f}\left(1+\frac{1}{\beta}\right)\left(\frac{\partial u}{\partial y}\right)^2+\frac{\sigma B^2(x,t)}{(\rho c)_f}u^2-\frac{1}{(\rho c)_f}\frac{\partial q_r}{\partial y}+\frac{Q(x,t)}{(\rho c)_f}(T-T_\infty), \tag{4}$$

$$\frac{\partial C}{\partial t}+u\frac{\partial C}{\partial x}+v\frac{\partial C}{\partial y}=D_B\frac{\partial^2 C}{\partial y^2}+\frac{D_T}{T_\infty}\frac{\partial^2 T}{\partial y^2}-k_c\,(C-C_\infty), \tag{5}$$

where u and v are the velocity components along the x and y directions respectively, ν_f is kinematic viscosity, ρ is the fluid density, σ is the electrical conductivity, β is the Casson parameter, φ is the porosity, $k_1(x,t)=k_0x^{1-n}(1-\varepsilon t)$ is the time dependent permeability of porous medium, k_0 is the permeability constant, g_x is the gravitational force due to acceleration, β_T is the coefficient of thermal expansion, β_C is the coefficient of concentration expansion, T is the fluid temperature, C is the nanoparticles concentration, $\alpha_f=\frac{k}{(\rho c)_f}$ is the thermal diffusivity of the Casson fluid, k is the thermal conductivity of the Casson fluid, c_f is the specific heat of fluid, $\tau=\frac{(\rho c)_p}{(\rho c)_f}$ is the ratio between the heat capacity of the nanoparticle material and heat capacity of the fluid, c_p is the specific heat of nanoparticles, D_B is the Brownian diffusion coefficient, D_T is the thermophoretic diffusion coefficient, q_r is the radiative heat flux, $Q(x,t)=\frac{Q_0x^{n-1}}{1-\varepsilon t}$ is heat generation or absorption coefficient, $k_c(x,t)=ak_2x^{n-1}(1-\varepsilon t)^{-1}$ is the variable rate of chemical reaction, k_2 is the constant reaction rate and a is the reference length along the flow. The ambient values of temperature and nanoparticles concentration are $T_\infty$and C_∞, respectively.

The corresponding boundary conditions are expressed as follows

$$t<0: \quad u=v=0, T=T_\infty, C=C_\infty, \text{ for any } x,\ y, \tag{6}$$

$$t\geq 0: \quad u=u_w(x,t)+N_1\nu_f\left(1+\frac{1}{\beta}\right)\frac{\partial u}{\partial y}, v=0,$$
$$k_f\frac{\partial T}{\partial y}=-h_f(T_f-T), D_B\frac{\partial C}{\partial y}=-h_s(C_s-C), \text{ at } y=0, \tag{7}$$
$$u\to 0, T\to T_\infty, C\to C_\infty, \text{ as } y\to\infty. \tag{8}$$

Here, $N_1(x,t)=N_0x^{-(n-1)/2}(1-\varepsilon t)^{1/2}$ denotes velocity slip with constant $N_0h_f(x,t)=h_0x^{(n-1)/2}(1-\varepsilon t)^{-1/2}$ and $h_s(x,t)=h_1x^{(n-1)/2}(1-\varepsilon t)^{-1/2}$ are the convective heat and mass transfer with h_0 and h_1 being constants. The wall of sheet is heated by temperature $T_f(x,t)=T_\infty+T_0x^{2n-1}(1-\varepsilon t)^{-2}$ with the reference temperature T_0. The nanoparticles concentration is denoted by $C_S(x,t)=C_\infty+C_0x^{2n-1}(1-\varepsilon t)^{-2}$ with C_0 being the reference concentration.

Following Roseland approximation, the radiative heat flux is defined as [25]

$$q_r=\frac{-4\sigma^*}{3k_1^*}\frac{\partial T^4}{\partial y}, \tag{9}$$

where σ^* is the Stefan-Boltzmann constant and k_1^* is the mean absorption coefficient. It is assumed that the temperature differences within the flow are sufficiently small such thatT^4can be expressed as linear function of temperature. Hence, expanding T^4 in Taylor series about T_∞ and neglecting higher order terms, we obtain the following

$$T^4 \cong 4T_\infty^3 T - 3T_\infty^4. \tag{10}$$

Substituting Eqs. (9) and (10) into Eq (4), we obtain

$$\frac{\partial T}{\partial t} + u\frac{\partial T}{\partial x} + v\frac{\partial T}{\partial y} = \alpha_f \left(1 + \frac{16\sigma^* T_\infty^3}{3k_f k^*}\right)\frac{\partial^2 T}{\partial y^2} + \tau\left[D_B \frac{\partial C}{\partial y}\frac{\partial T}{\partial y} + \frac{D_T}{T_\infty}\left(\frac{\partial T}{\partial y}\right)^2\right] + \frac{\nu_f}{c_f}\left(1 + \frac{1}{\beta}\right)\left(\frac{\partial u}{\partial y}\right)^2 + \frac{\sigma B^2(x,t)}{(\rho c)_f}u^2 + \frac{Q(x,t)}{(\rho c)_f}(T - T_\infty). \tag{11}$$

Now, the following similarity transformations applied by Mukhopadhyay [20] and Ibrahim *et al.* [26] are introduced to convert the partial differential equations into ordinary differential equations;

$$\begin{aligned} \psi &= \sqrt{\frac{2\nu_f c}{(n+1)(1-\varepsilon t)}}x^{(n+1)/2} f(\eta), \quad \eta = \sqrt{\frac{(n+1)c}{2\nu_f(1-\varepsilon t)}}x^{(n-1)/2} y, \\ \theta &= \frac{T - T_\infty}{T_f - T_\infty}, \qquad\qquad \phi = \frac{C - C_\infty}{C_S - C_\infty}, \end{aligned} \tag{12}$$

where η is the local similarity variable, ψ is the stream function, $f(\eta)$ is the dimensionless stream function, $\theta(\eta)$ is a dimensionless temperature of the fluid in the boundary layer region and $\phi(\eta)$ is a dimensionless concentration of the fluid in the boundary layer region.

The continuity equation (2) is satisfied by introducing the stream function ψ such that

$$u = \frac{\partial \psi}{\partial y}, \quad v = -\frac{\partial \psi}{\partial x}. \tag{13}$$

Using equation (12), the governing Eqs. (3), (5) and (11) are reduced to the following non-dimensional equations

$$\left(1 + \frac{1}{\beta}\right)f''' + ff'' - \frac{2n}{n+1}(f')^2 - \left(M + \left(1 + \frac{1}{\beta}\right)K\right)f' + \lambda(\theta - N\phi) - A\left(\frac{2}{n+1}f' + \frac{1}{n+1}\eta f''\right) = 0, \tag{14}$$

$$\frac{1}{\Pr}\left(1 + \frac{4}{3}R_d\right)\theta'' + f\theta' - \frac{2(2n-1)}{n+1}f'\theta + \left(1 + \frac{1}{\beta}\right)Ec(f'')^2 + MEc(f')^2 + \gamma\theta + N_b\phi'\theta' + N_t(\theta')^2 - A\left(\frac{4}{n+1}\theta + \frac{1}{n+1}\eta\theta'\right) = 0, \tag{15}$$

$$\frac{1}{Le}\phi'' + f\phi' - \frac{2(2n-1)}{n+1}f'\phi + \frac{N_t}{N_b}\theta'' - \frac{2}{n+1}R\phi - A\left(\frac{4}{n+1}\phi + \frac{1}{n+1}\eta\phi'\right) = 0, \tag{16}$$

subject to the boundary conditions

$$f(0)=0,\quad f'(0)=1+\delta\sqrt{\frac{n+1}{2}}\left(1+\frac{1}{\beta}\right)f''(0),$$

$$\theta'(0)=-\left(\sqrt{\frac{2}{n+1}}\right)Bi_1\left[1-\theta(0)\right],\quad \phi'(0)=-\left(\sqrt{\frac{2}{n+1}}\right)Bi_2\left[1-\phi(0)\right], \tag{17}$$

$$f'(\infty)=0,\quad \theta(\infty)=0,\quad \phi(\infty)=0, \tag{18}$$

where prime denotes differentiation with respect to η.The physical parameters involved in the above expressions are the local unsteadiness parameter A, magnetic parameter M, porosity parameter K, thermal buoyancy parameter $\lambda=\pm\frac{Gr_x}{Re_x^2}$ where Gr_x and Re_x are Grashof number and local Reynold number respectively in which $\lambda>0$ denotes the assisting flow, $\lambda=0$ indicates no convection and $\lambda<0$ corresponds the opposing flow, buoyancy ratio parameter N, slip parameterδ, Prandtl numberPr, radiation parameter R_d, Eckert number Ec, heat generation /absorption parameter γ, Brownian motion parameterN_b, thermophoresis parameter N_t Biot numbers Bi_1 and Bi_2, Lewis number Le and chemical reaction parameter R, and are defined as

$$A=\frac{\varepsilon x}{cx^n},\ M=\frac{2\sigma B_0^2}{\rho_f c\,(n+1)},\ K=\frac{2\nu_f\varphi}{k_0 c\,(n+1)},\ Gr_x=\frac{2g_x\beta_T\left(T_f-T_\infty\right)x^3}{\nu_f^2\,(n+1)},$$

$$Re_x=\frac{xu_w}{\nu_f},\ N=\frac{\beta_c\left(C_s-C_\infty\right)}{\beta_T\left(T_f-T_\infty\right)},\ \delta=N_0\sqrt{c\nu_f},\ \mathrm{Pr}=\frac{\nu_f}{\alpha_f},\ R_d=\frac{4\sigma^*T_\infty^3}{k_f k_1^*},$$

$$Ec=\frac{u_w^2}{c_f\left(T_f-T_\infty\right)},\ \gamma=\frac{2Q_0}{\rho c_f\,(n+1)\,c},\ N_b=\frac{\tau D_B\left(C_S-C_\infty\right)}{\nu_f},\ N_t=\frac{\tau D_T\left(T_f-T_\infty\right)}{\nu_f T_\infty},$$

$$Bi_1=\frac{h_0}{k}\left[\frac{\nu_f}{c}\right]^{1/2},\ Bi_2=\frac{h_1}{D_B}\left[\frac{\nu_f}{c}\right]^{1/2},\ Le=\frac{\nu_f}{D_B},\ R=\frac{\nu_f a k_2}{c}.$$

The physical quantities of interest which govern the flow are the local skin friction coefficient Cf_x, local Nusselt number Nu_x and local Sherwood number Sh_x, which are defined as

$$Cf_x=\frac{\tau_w}{\rho_f u_w^2},\quad Nu_x=\frac{xq_w}{\alpha_f\left(T_f-T_\infty\right)},\quad Sh_x=\frac{xq_s}{D_B\left(C_S-C_\infty\right)},$$

where τ_w, q_w and q_s are the wall skin friction, wall heat flux and wall mass flux respectively given by

$$\tau_w=\mu_B\left(1+\frac{1}{\beta}\right)\left[\frac{\partial u}{\partial y}\right]_{y=0},\quad q_w=-\left(\left(\alpha_f+\frac{16\sigma^*T_\infty^3}{3\left(\rho c\right)_f k_1^*}\right)\frac{\partial T}{\partial y}\right)_{y=0},\quad q_s=-D_B\left(\frac{\partial C}{\partial y}\right)_{y=0}.$$

The dimensionless forms of the skin friction coefficient, local Nusselt number, and local Sherwood number are

$$\left(Re_x\right)^{1/2}Cf_x=\sqrt{\tfrac{n+1}{2}}\left(1+\tfrac{1}{\beta}\right)f''(0),$$

$$\left(Re_x\right)^{-1/2}Nu_x=-\sqrt{\tfrac{n+1}{2}}\left(1+\tfrac{4}{3}R_d\right)\theta'(0),$$

$$\left(Re_x\right)^{-1/2}Sh_x=-\sqrt{\tfrac{n+1}{2}}\phi'(0),$$

where Re_x is the local Reynolds number based on the stretching velocity u_w.

3 Numerical Scheme

The nonlinear coupled ordinary differential equations (14) to (16) with associated boundary conditions (17) and (18) are solved numerically using implicit finite difference scheme known as Keller box method. This method is unconditionally stable with a second order convergence. It is also found to be very suitable in dealing with nonlinear parabolic problems. The details of this method are described in the book by Cebeci and Bradshaw [27]. The Keller box method comprises the following four steps that need to be done in order to obtain the numerical solutions. The four steps involved are as follows:

1. The ordinary differential equations are reduced to a system of first order equations.
2. The first order system is discretized into finite difference form by using central difference scheme.
3. The system of equations is linearized using Newton's method and then written in matrix-vector form.
4. Finally, the linear system can be solved via block tri-diagonal elimination technique.

4 Results and Discussion

The governing nonlinear differential equations (14) to (16) subject to boundary conditions (17) and (18) are computed numerically via Keller-box method. An algorithm is developed in MATLAB software in order to generate numerical and graphical results. Further, it is necessary to make suitable guess for the step size $\Delta\eta$ and boundary layer thickness η_∞. In the present study, $\Delta\eta = 0.01$ and $\eta_\infty = 10$are used. The iteration process is repeated until the convergence criteria 10^{-5} is satisfied [28].

In order to analyze the behavior of velocity, temperature and concentration profiles, numerical calculations are carried out for various values A, β, n, M, K, λ, N, Pr, Ec, γ, R_d, N_b, N_t, Le, R, δ, Bi_1 and Bi_2. For validation of the present algorithm developed in MATLAB software, the numerical results for skin friction coefficient and local Nusselt number are compared with previous published results as limiting cases and presented in Tables 1 and 2.

Table 1 displays the comparison of skin friction coefficient for different values ofβ and M with the results of Nadeem *et al.* [29] and Ullah *et al.* [23]. The results showed an excellent agreement. In Table 2, the present results of reduced Nusselt number are compared with the results of Yih [30], Aurangzaib *et al.* [31] and Pal *et al.* [32] for various values of Pr and revealed in a good agreement.

Figures 1 to 3 are plotted to analyze dimensionless velocity profile for various effects of A, β and n. Figure 1 reveals the effect of Aon fluid velocity for $\beta = 0.6$ (Casson fluid) and $\beta \to \infty$ (Newtonian fluid). It is noteworthy here that $A = 0$ and $A \neq 0$ represent the steady and unsteady case respectively. It is found that fluid velocity reduces as A increases for both fluids. It is also observed that the momentum boundary layer becomes thinner for larger amplitude of A. The variation of β on fluid velocity when $\lambda < 0$, $\lambda = 0$ and $\lambda > 0$ is displayed in Figure 2. It is significant that the present problem reduces to pure Newtonian nanofluidwhen $\beta \to \infty$. Clearly, fluid velocity decelerates with increase in β. The reason behind this behavior is that

Table 1: Comparison of Skin Friction Coefficient for Different Values of β and M when $n = 1$, $\beta \to \infty$, $Bi_1 \to \infty$, $Bi_2 \to \infty$ and $A = K = \lambda = N = \delta = R_d = Le = N_t = N_b = R = 0$

$-\left(1+\frac{1}{\beta}\right) f''(0)$				
β	M	Nadeem *et al.* [29]	Ullah*et al.* [23]	Present results
∞		1.0042	1.0000	1.0000
5		1.0954	1.0955	1.0955
1		1.4142	1.4144	1.4144
∞	10	3.3165	3.3166	3.3166
5		3.6331	3.6332	3.6332
1		4.6904	4.6904	4.6904
∞	100	10.0498	10.0499	10.0499
5		11.0091	11.0091	11.0091
1		14.2127	14.2127	14.2127

Table 2: Comparison of $-\theta'(0)$ for Different Pr with $n = 1$, $\beta \to \infty Bi_1 \to \infty$,,$Bi_2 \to \infty$ and $A = M = K = \lambda = N = \delta = R_d = Le = N_t = N_b = R = 0$

$-\theta'(0)$				
Pr	Yih[30]	Aurangzaib*et al.* [31]	Pal *et al.* [32]	Present results
0.72	0.8086	0.8086	0.8086	0.8088
1	1.0000	1.0000	1.0000	1.0000
3	1.9237	1.9237	1.9237	1.9237
10	3.7207	3.7207	3.7206	3.7208
100	12.2940	12.3004	12.2939	12.3003

higher values of β increase the plasticity of fluid that cause the fluid to become more viscous. Consequently, the momentum boundary layer thickness reduces as β increases. It is also noticed that momentum boundary thickness reduces faster in case of opposing flow ($\lambda < 0$) compared to assisting flow ($\lambda > 0$) when β approaches infinity. The effect of n on velocity profile for both steady and unsteady cases is plotted in Figure 3. In both cases, fluid velocity is found as increasing functions of n. It is seen that the momentum boundary layer thinning rapidly when $A \neq 0$

Figures 4 to 10 exhibit the variation of dimensionless temperature profile for various values of A, β, $n\gamma$, R_d, N_b and N_t. Figure 4 shows the influence of A on temperature profile for $M = 0$ and $M \neq 0$. It can be seen that increasing values of A lead to reduction in fluid temperature and thermal boundary layer thickness. It is clear from Figure 5 that fluid temperature increases with the increase in β for both cases of $n = 1$ and $n \neq 1$. This phenomenon indicates that increasing β implies a reduction in yield stress. It is well-known fact that yield stress decreases with an increase in temperature. Figure 6 illustrates the effect of n on temperature profile for $M = 0$ and $M \neq 0$. It is observed that fluid temperature decreases as n increases. The thermal

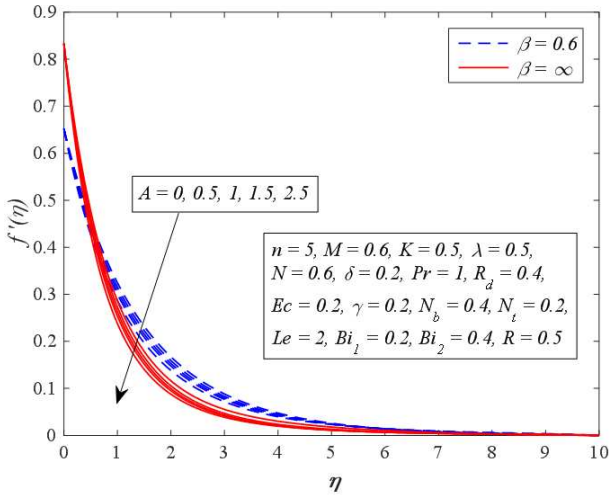

Figure 1: Effect of A on Velocity for Different Values of β

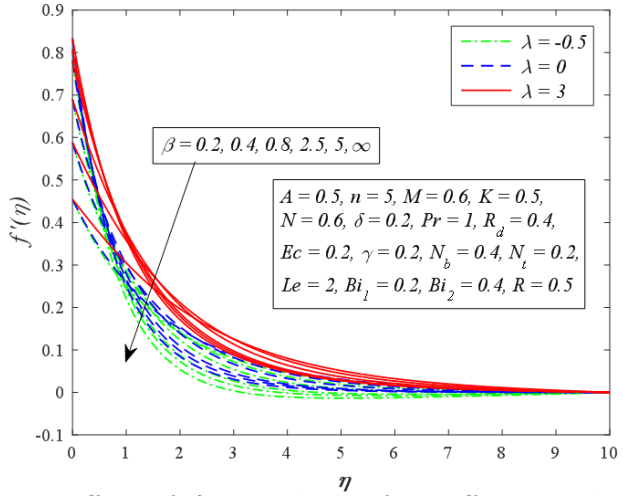

Figure 2: Effect of β on Velocity for Different Values of λ

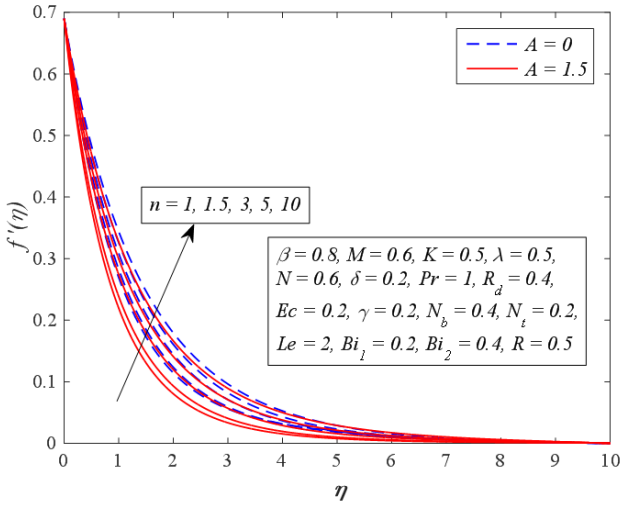

Figure 3: Effect of n on Velocity for Different Values of A

boundary layer is thinner when the sheet is stretched in a nonlinear way ($n \neq 1$) compared to linear way ($n = 1$). The effect of R_d on temperature profile for $n = 1$ and $n \neq 1$ is illustrated in Figure 7. It is worth to mention that $R_d = 0$ shows no radiation and $R_d \neq 0$ denotes the presence of thermal radiation. It is noticed that temperature of fluid rises as R_d increases. The reason is that increasing R_d values enhance the heat energy transferred to the fluid and this result increase in thermal boundary layer thickness. The influence of γ on temperature profile for $A = 0$ and $A \neq 0$ is shown in Figure 8. It is important to note that $\gamma > 0$ corresponds to heat generation and $\gamma < 0$represent heat absorption. It can be seen that temperature increases when $\gamma > 0$, whereas it decreases when $\gamma < 0$. The existence of heat source causes an increase in thermal energy of fluid resulting in the enhancement of fluid temperature and thickens the thermal boundary layer. Also, an opposite behavior is observed in which thermal boundary layer thickness reduces in the presence of heat absorption. Figure 9 demonstrates the effect of N_b on temperature profile for $M = 0$ and $M \neq 0$. It is found that temperature is an increasing function ofN_b. It is an agreement with the fact that Brownian motion of nanoparticles that occurs in nanofluid systems contributes to the enhancement of the thermal conductivity. Hence, increasing N_b leads to increase in heat transfer properties and resulting in higher temperature of nanofluids. The variation of temperature profile for different values of N_t when $M = 0$ and $M \neq 0$ is presented in Figure 10. It is found that fluid temperature slightly increases with increment in N_t. This is due to the fact that larger values of N_t mplies higher temperature differences between hot surface and ambient fluid. The presence of temperature gradient imposes thermophoretic force on nanoparticles. Hence, thermophoretic force elevates the disperse of nanoparticles from the hot surface to the ambient fluid which results in enhancing fluid temperature.

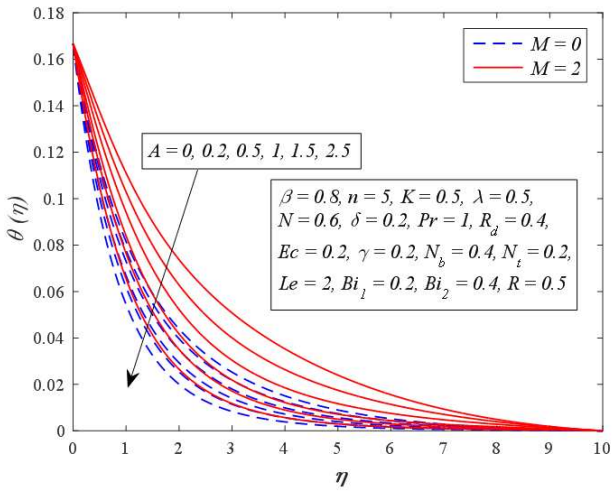

Figure 4: Effect of A on Temperature for Different Values of M

Figures 11 to 16 examine the variation of nanoparticles concentration profile for various values of A, β, nN_b, N_t and R. Figure 11 presents the effect of A on nanoparticles concentration profile when $n = 1$ and $n \neq 1$. In both cases, concentration of nanoparticles drops as A increases. A reduction in concentration boundary layer thickness is also observed. The influence of A on concentration profile is more significant for nonlinear stretching sheet case. The influence of β on nanoparticles concentration profile in both cases of $A = 0$ and $A \neq 0$

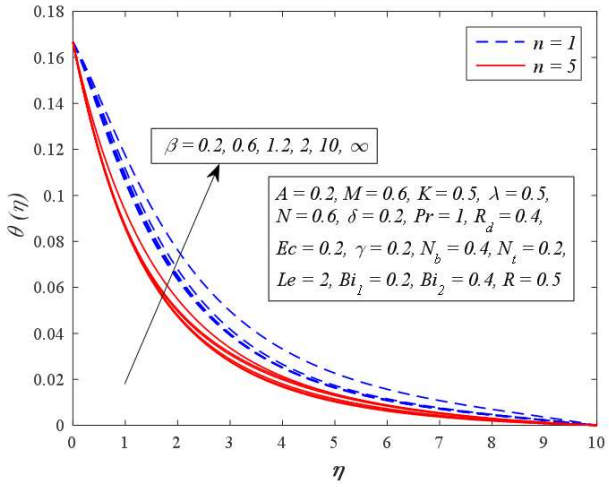

Figure 5: Effect of β on Temperature for Different Values of$n$

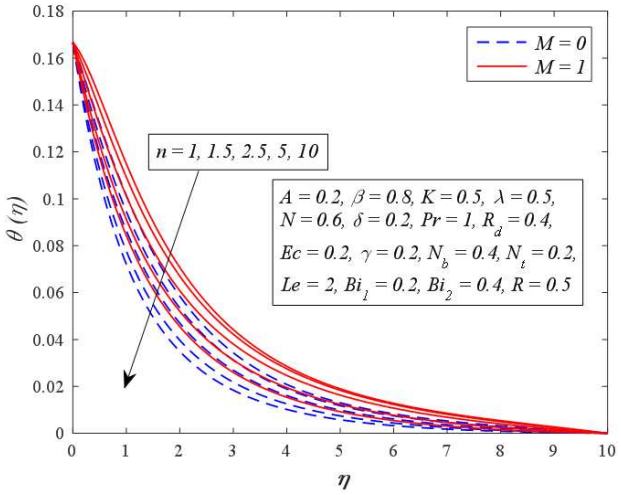

Figure 6: Effect of n on Temperature for Different Values of M

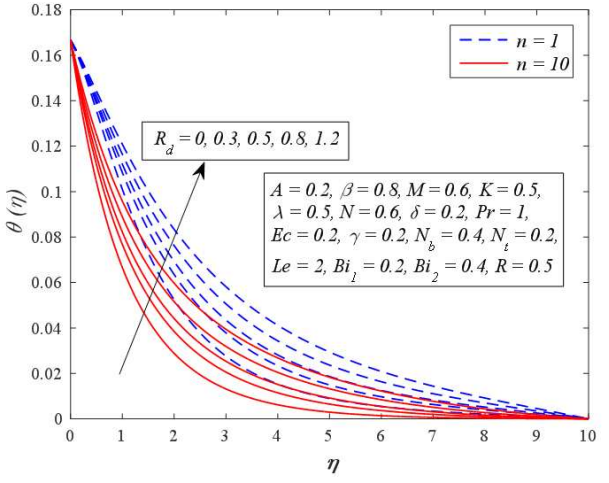

Figure 7: Effect of R_d on Temperature for Different Values of n

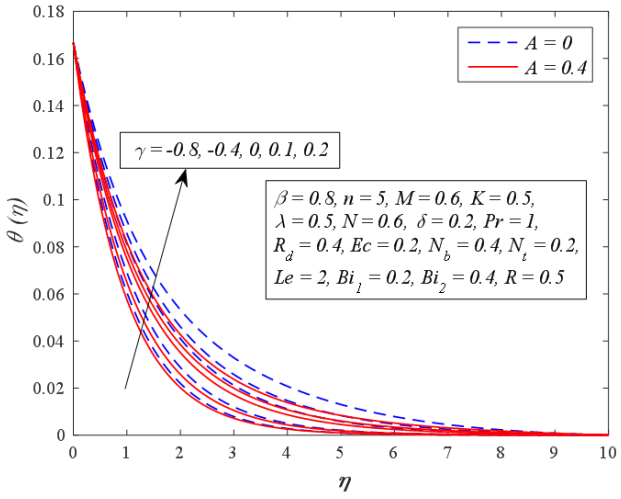

Figure 8: Effect of γ on Temperature for Different Values of A

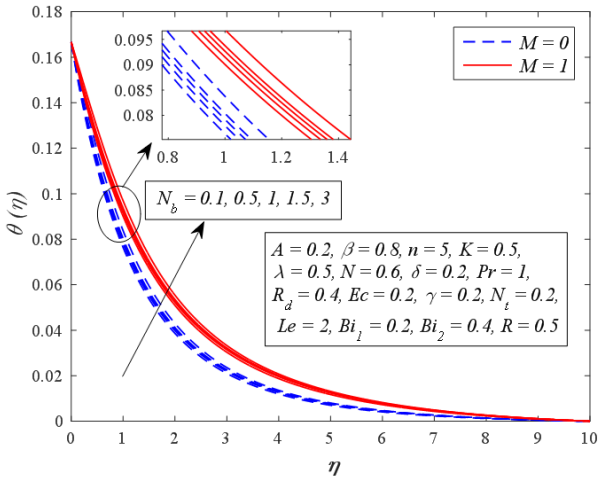

Figure 9: Effect of N_b on Temperature for Different Values of M

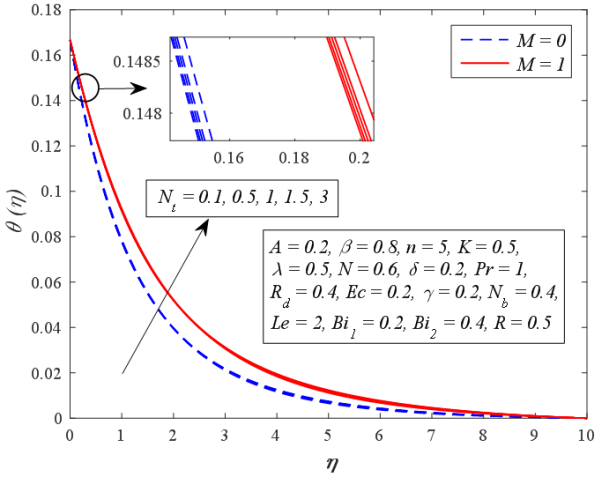

Figure 10: Effect of N_t on Temperature for Different Values of M

is portrayed in Figure 12. It is noticed that nanoparticles concentration is slightly enhanced with increase in β. Figure 13 displays that nanoparticles concentration declines as n increases for $K = 0$ and $K \neq 0$. Consequently, the thickness of concentration boundary layer reduces when $n > 1$. Figure 14 exhibits that nanoparticles concentration falls as N_b increases in both cases of $M = 0$ and $M \neq 0$. It is well-known fact that Brownian motion is a diffusion process. The enhancement of N_b promotes the diffusion rate, and as consequence, the thermal conductivity becomes higher. Moreover, the nanoparticles raise the sheet surface area for heat transfer. The increment in random motion of nanoparticles increases the kinetic energy which lead to reduction in nanoparticles concentration. The influence of N_t on nanoparticles concentration profile for $M = 0$and $M \neq 0$is shown in Figure 15. It is noted that larger values of N_t increases the nanoparticles concentration. Physically, the existence of thermophoretic force on nanofluid due to temperature gradient enhances heat transfer from the hot surface to the moving fluid and apparently thinning the concentration boundary layer. Figure 16 illustrates the variation of R on nanoparticles concentration when $A = 0$ and $A \neq 0$. It is found that nanoparticles concentration slightly increases in the case of generative chemical reaction ($R < 0$), while it drops in the case of destructive chemical reaction ($R > 0$). The explanation for this behavior is that the mass transfer rate decreases when $R < 0$, which leads to an increment in nanoparticle concentration. A decrease in thickness of concentration boundary layer is also observed. Meanwhile, opposite effect is seen for destructive chemical reaction.

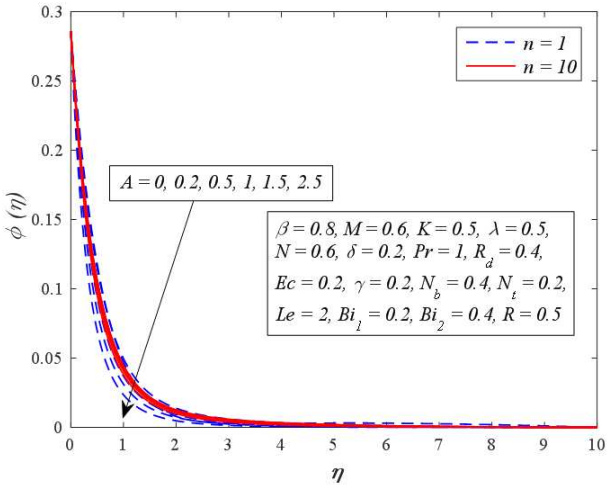

Figure 11: Effect of A on Nanoparticles Concentration for Different$n$

Figures 17 to 21 depict the variation of skin friction coefficient, local Nusselt number and local Sherwood number for various values of A, β, K, λ, n, δ, R_d, Pr, N_b, N_t, M, Le and R, respectively. Figure 17 presents the influence of skin friction coefficient for different values of A, β and K. It is observed that the wall shear stress declines with increase in A and K, whereas opposite effect is shown when β increases. The impact of unsteadiness and porous medium parameter reduces the fluid flow which causes the momentum boundary layer thickness decreases and consequently enhances the friction between fluid and solid surface. It is noticeable that skin friction coefficient is negative for all values of A, β and K because the fluid experiences a drag force from nonlinear stretching sheet. The effect of λ, n and δ on skin friction coefficient is displayed in Figure 18. It is found that increasing values of λ and δ enhances the wall shear

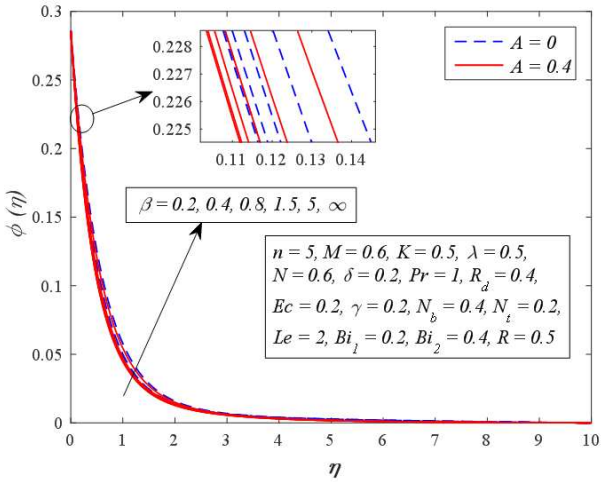

Figure 12: Effect of β on Nanoparticles Concentration for Different A

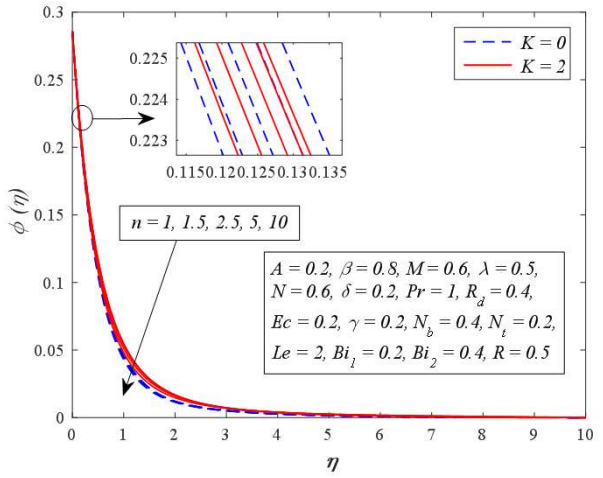

Figure 13: Effect of n on Nanoparticles Concentration for Different K

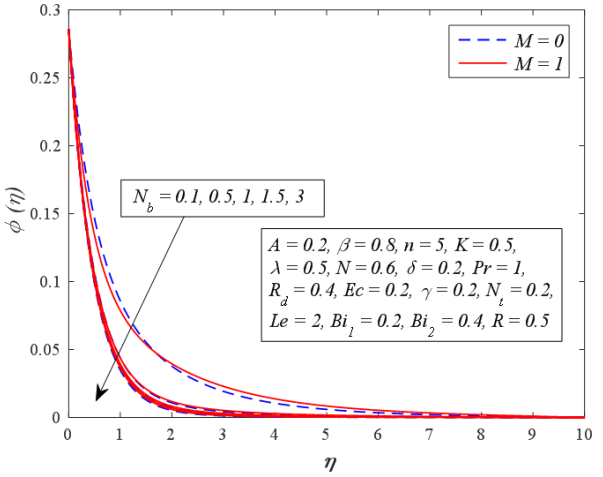

Figure 14: Effect of N_b on Nanoparticles Concentration for Different M

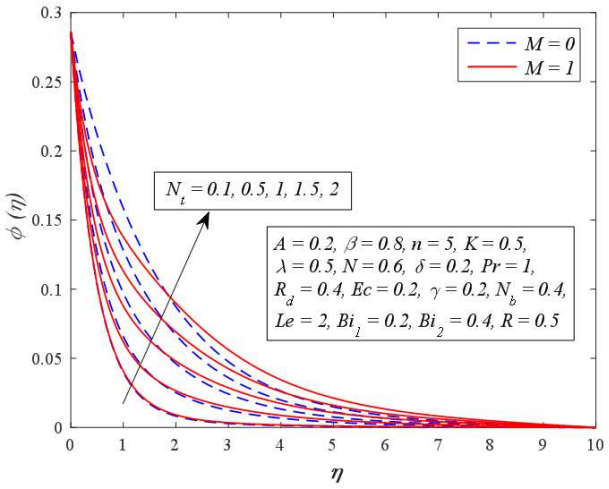

Figure 15: Effect of N_t on Nanoparticles Concentration for different M

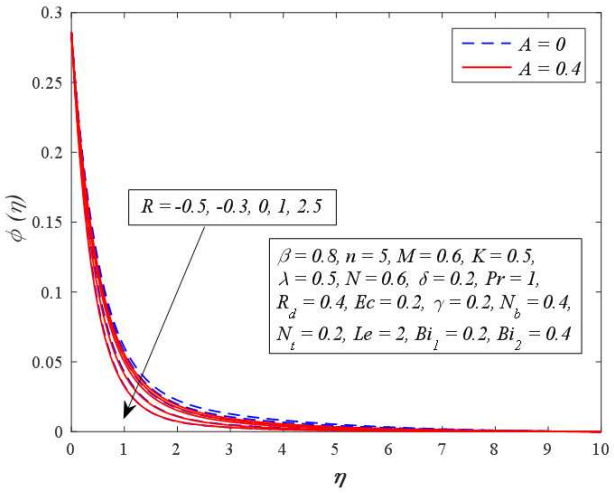

Figure 16: Effect of R on Nanoparticles Concentration for Different A

stress, while the increment of n results in the wall shear stress rises when $\lambda < 0$ and it reduces when $\lambda > 0$. Figure 19 demonstrates the influence of β, δ and R_d on local Nusselt number. It is observed that β and R_d boost the heat rate transfer, whereas it drops as δ increases. The variation of local Nusselt number for different values of Pr, N_b and N_t are portrayed in Figure 20. The heat rate transfer declines with increase in N_b and N_t, while it rises with the increment of Prandtl number. Since the strength of Brownian motion and thermophoresis enhances the thermal conductivity of base fluid, it led to reduction in the temperature gradient for both parameters. Finally, the effect of M, Le and R on local Sherwood number is illustrated in Figure 21. It is noticed that mass transfer rate rises for increasing values of Le and R, whereas it slightly reduces with increase in M

5 Conclusions

The present study investigates numerical results of unsteady MHD mixed convection flow of Cassonnano fluid over nonlinearly stretching sheet immersed in a porous medium in the

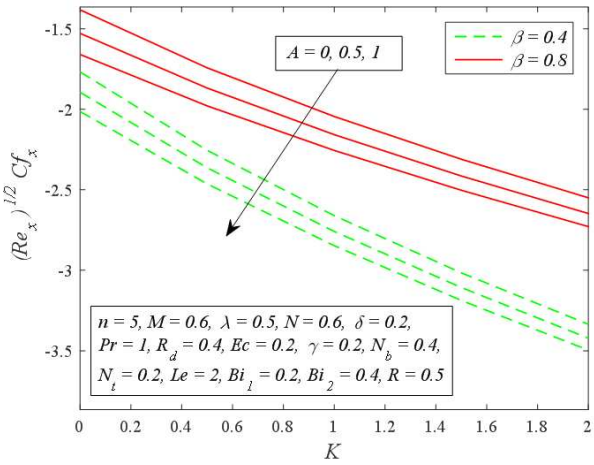

Figure 17: Variation of Skin Friction Coefficient for Various Values of A, β and K

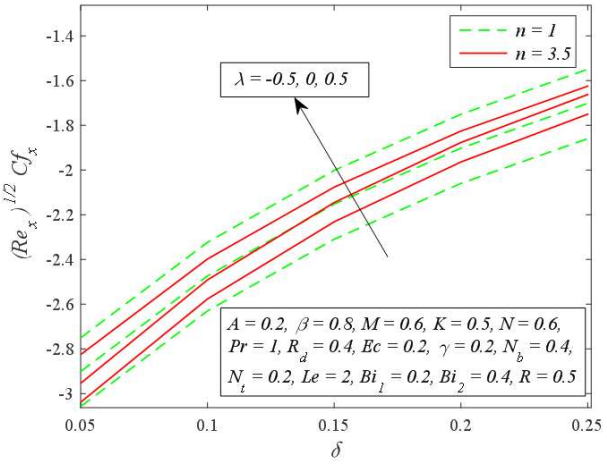

Figure 18: Variation of Skin Friction Coefficient for Various Values of λ, n and δ

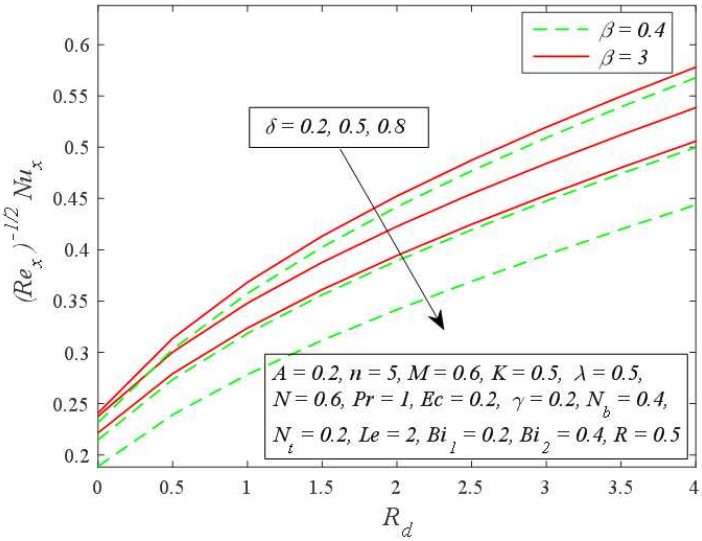

Figure 19: Variation of Nusselt Number for Various Values of δ, $\beta$and R_d

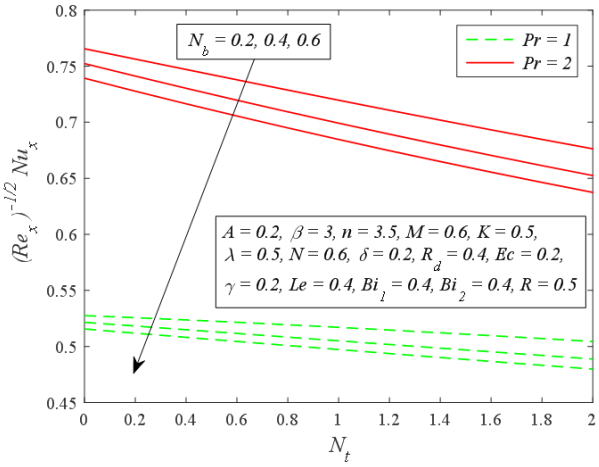

Figure 20: Variation of Nusselt Number for Various Values of N_b,Pr and N_t

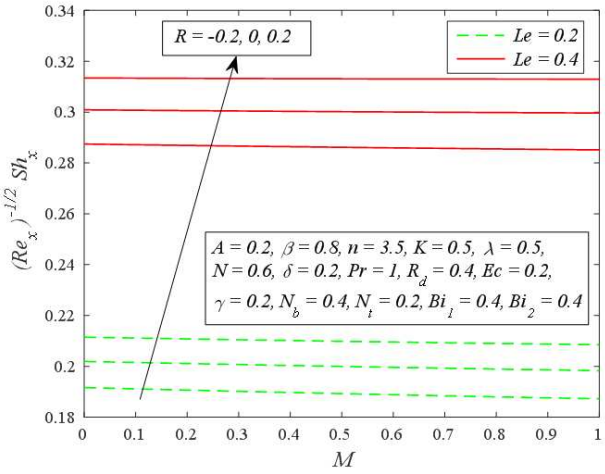

Figure 21: Variation of Sherwood Number for Various Values of R,Le and M

presence of chemical reaction, thermal radiation and heat generation/absorption. Moreover, the influence of viscous dissipation, joule heating, slip and convective boundary conditions are also considered. Similarity transformations are used for the conversion of nonlinear partial differential equations to nonlinear ordinary differential equations. The resulting equations are solved numerically via Keller box method. Numerical and graphical results are obtained through MATLAB software. In order to check the validity of the present method, the numerical solutions for wall shear stress and heat transfer rate are compared with the results of existing literature and excellent accuracy is achieved from both results. The effect of physical parameters, namely, local unsteadiness parameter A, Casson parameterβ, nonlinear stretching parameter n, magnetic parameter M, porosity parameter K, thermal buoyancy parameter λ, buoyancy ratio parameter N, Prandtl number Pr, radiation parameter R_d, Eckert number Ec, heat generation or absorption parameterγ, Brownian motion parameterN_b, thermophoresis parameter N_t Lewis number Le, chemical reaction parameter R, slip parameter δ and Biot numbers Bi_1, Bi_2 on fluid velocity, temperature, concentration as well as wall shear stress, heat and mass transfer rates are presented graphically and analyzed. The main findings of present study can be deduced as

follows:

1. The fluid velocity is a decreasing function of unsteadiness parameter.
2. The magnitude of wall shear stress and heat transfer rate rises for increasing values of β
3. The fluid velocity reduces whereas both temperature and nanoparticles concentration rise with increment in β
4. The fluid velocity increases in the case of assisting flow ($\lambda > 0$), while it decreases in the case of opposing flow($\lambda < 0$).
5. The heat transfer rate enhances with increase in R_d
6. The concentration boundary layer becomes thinner due to destructive chemical reaction ($R > 0$).
7. The enhancement of $N_t$boosts temperature and nanoparticles concentration.

Acknowledgments

The author would like to acknowledge Ministry of Education (MOE) and Research Management Centre of Universiti Teknologi Malaysia (UTM) for the financial support through vote number 07G77 for this research.

References

[1] Choi, S. U. S., and Eastman, J. A. Enhancing thermal conductivity of fluids with nanoparticles. *ASME-Publications-Fed*. (1995). 231: 99–106.

[2] Xuan, Y., and Roetzel, W. Conceptions for heat transfer correlation of nanofluids. *International Journal of Heat and Mass Transfer*. (2000). 43(19): 3701–3707.

[3] Xuan, Y., and Li, Q. Heat transfer enhancement of nanofluids. *International Journal of Heat and Fluid Flow*. (2000). 21(1): 58–64.

[4] Wong, K. V., and De Leon, O. Applications of nanofluids: current and future. *Advances in MechanicalEngineering.*(2010).

[5] Buongiorno, J. Convective Transport in Nanofluids. *ASME J. of Heat Transfer.*(2006).128(3): 240–250.

[6] Anwar, M. I., Shafie, S., Khan, I., and Salleh, M. Z. Conjugate effects of radiation flux on double diffusive MHD free convection flow of a nanofluid over a power law stretching sheet. *International Scholarly Research Network*. (2012). 1–7.

[7] Hayat, T., Ashraf, M. B., Shehzad, S. A., and Alsaedi, A. Mixed convection flow of Casson nanofluid over a stretching sheet with convectively heated chemical reaction and heat source/sink. *Journal of Applied Fluid Mechanics.*(2014). 8(4): 803–813.

[8] Daniel, Y. S., Aziz, A. Z., Zuhaila, I., and Salah, F. Entropy analysis in electrical magnetohydrodynamic (MHD) flow of nanofluid with effects of thermal radiation, viscous dissipation and chemical reaction. *Theoretical & Applied Mechanics Letters.*(2017). 7(4): 235–242.

[9] Crane, L. J. Flow past a stretching plate. *Zeitschrift für angewandte Mathematik und Physik (ZAMP).* (1970). 21(4): 645–647.

[10] Gupta, A., and Gupta, P. Heat and mass transfer on a stretching sheet with suction or blowing. *The Canadian Journal of Chemical Engineering.*(1977). 55(6): 744–746.

[11] Kumaran, V., and Ramanaiah, G. A note on the flow over a stretching sheet. *Acta Mech.* (1996).116: 229–233.

[12] Magyari E., and Keller, B. Heat and mass transfer in the boundary layers on an exponentially stretching continuous surface. *J Phys D Appl Phys.* (1999). 32: 577–585.

[13] Cortell, R. Viscous flow and heat transfer over a nonlinearly stretching sheet. *Applied Mathematics and Computation.* (2007). 184(2): 864–873.

[14] Hsiao, K. Mixed convection with radiation effect over a nonlinearly stretching sheet. *World Academy of Science, Engineering and Technology.* (2010). 4(2): 338–342.

[15] Sharidan, S., Mahmood, T., and Pop, I. Similiarity solutions for the unsteady boundary layer flow and heat transfer due to a stretching sheet. *Int. J. of Applied Mechanics and Engineering.* (2006). 11(3): 647–654.

[16] Bachok, N., Ishak, A., and Pop, I. Unsteady boundary-layer flow and heat transfer of a nanofluid over a permeable stretching/shrinking sheet. *International Journal of Heat and Mass Transfer.* (2012). 55(7–8): 2102–2109.

[17] Mustafa, M., Hayat, T., and Alsaedi, A. Unsteady boundary layer flow of nanofluid past an impulsively stretching sheet. *Journal of Mechanics.* (2013). 29(3): 423–432.

[18] Ullah, I., Shafie, S., and Khan, I. Soret and Dufour effects on unsteady mixed convection slip flow of Casson fluid over a nonlinearly stretching sheet with convective boundary condition. *Scientific Reports.*(2017). 7.

[19] Casson, N. A flow equation for pigment-oil suspensions of the printing ink type. *In: Mill, C.C., Ed., Rheology of Disperse Systems, Pergamon Press, Oxford.* (1959). 84–104.

[20] Mukhopadhyay, S. Casson fluid flow and heat transfer over a nonlinearly stretching surface. *Chinese Physics B.* (2013). 22(7).

[21] Sumalatha, C., and Bandari, S. Effects of radiations and heat source/sink on a Casson fluid flow over nonlinear stretching sheet. *World Journal of Mechanics.* (2015). 5: 257–265.

[22] Oyelakin, I. S., Mondal, S., and Sibanda, P. Unsteady Casson nanofluid flow over a stretching sheet with thermal radiation, convective and slip boundary conditions. *Alexandria Engineering Journal.*(2016). 55(2): 1025–1035.

[23] Ullah, I., Bhattacharyya, K., Shafie, S., and Khan, I. Unsteady MHD mixed convection slip flow of Casson fluid over nonlinearly stretching sheet embedded in a porous medium with chemical reaction, thermal radiation, heat generation/absorption and convective boundary conditions. *PLOSE One.*(2016). 11(10).

[24] Pramanik, S. Casson fluid flow and heat transfer past an exponentially porous stretching surface in presence of thermal radiation. *Ain Shams Engineering Journal*. (2014). 5(1): 205–212.

[25] Prasad, K. V., Datti, P. S., and Vajravelu, K. MHD mixed convection flow over a permeable non-isothermal wedge. *Journal of King Saud University–Science*. (2013). 25(4): 313–324.

[26] Ibrahim, S. M., Lorenzini, G., Kumar, V. P., and Raju, C. S. K. Influence of chemical reaction and heat source on dissipative MHD mixed convection flow of a Casson nanofluid over a nonlinear permeable stretching sheet. *International Journal of Heat and Mass Transfer*. (2017). 111: 346–355.

[27] Cebeci, T., and Bradshaw, P. *Physical and computational aspects of convective heat transfer* (1st ed.). New York: Springer New York. (1984).

[28] Ullah, I., Shafie, S., and Khan, I. Heat generation and absorption in MHD flow of Casson fluid past a stretching wedge with viscous dissipation and newtonian heating. *Jurnal Teknologi*. (2018). 80(3): 77–85.

[29] Nadeem, S., Haq, R. U., Akbar, N. S., and Khan, Z. H. MHD three dimensional Casson fluid flow past a porous linearly stretching sheet. *Alexandria Engineering Journal*. (2013). 52(4): 577–582.

[30] Yih, K. A. MHD forced convection flow adjacent to a non-isothermal wedge. *International Communications in Heat and Mass Transfer*. (1999). 26(6): 819–827.

[31] Aurangzaib, Kasim, A. R. M., Mohammad, N. F., and Shafie, S. Effect of thermal stratification on MHD free convection with heat and mass transfer over an unsteady stretching surface with heat source, Hall current and chemical reaction. *International Journal of Advances in Engineering Sciences and Applied Mathematics.*(2012).4(3): 217–225.

[32] Pal, D., Mandal, G. and Vajravalu, K. Soret and Dufour effects on MHD convective radiative heat and mass transfer of nanofluids over a vertical nonlinear stretching/shrinking sheet. *Applied Mathematics and Computation*. (2016). 287: 184–200.